Supplement of Atmos. Chem. Phys., 25, 13019–13035, 2025 https://doi.org/10.5194/acp-25-13019-2025-supplement © Author(s) 2025. CC BY 4.0 License.





Supplement of

Surface-bulk photochemical coupling of nonanoic acid and 4-benzoylbenzoic acid: the dual role of the photosensitizer and environmental influences

Ahmed Abdelmonem et al.

Correspondence to: Ahmed Abdelmonem (ahmed.abdelmonem@kit.edu)

The copyright of individual parts of the supplement might differ from the article licence.

S1. Photochemical reactor details

- 2 The illumination head of the custom-built Atmospheric Surface-Science Solar Simulator consists of
- 3 29 surface-mounted device (SMD) LEDs covering 18 central wavelengths between ~275 nm and
- 4 ~525 nm. Each LED type is driven by a dedicated current source, ensuring precise control over
- 5 spectral output. The spatial distribution of the LEDs was optimized, on a curved surface, for a uniform
- 6 illumination using a calibrated spectrophotometer (OCEAN Optics USB2000+).
- 7 Figure S1 illustrates the dimensions of the illumination head, while Fig. S2 shows the number and
- 8 spatial distribution of the LEDs on the spherical cap matrix of the photochemical reactor. Figure S3
- 9 provides a schematic of the sample illumination and ray geometry in the sum-frequency generation
- 10 (SFG) setup.

11

12

13

14

1

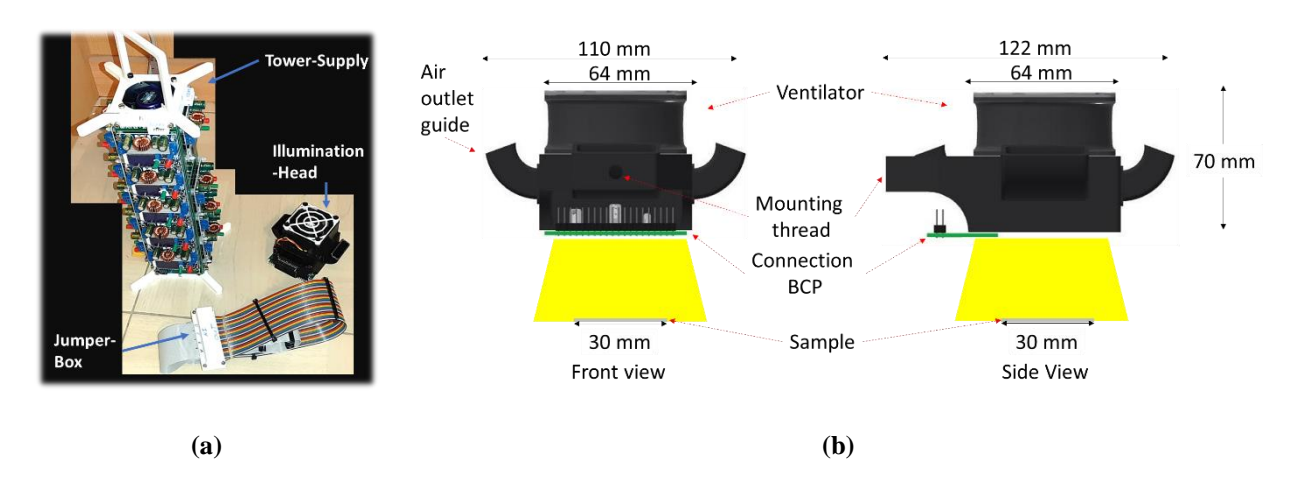


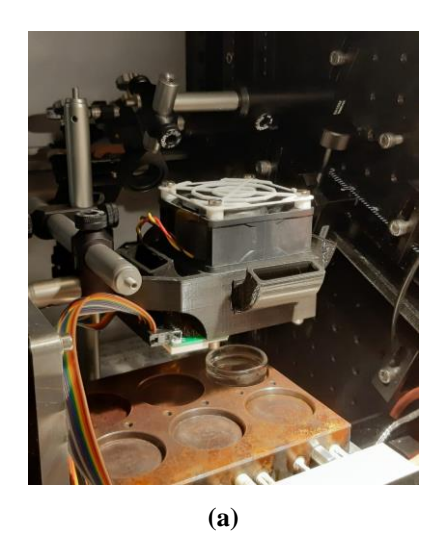
Figure S1: (a) A Photograph of the custom-built compact solar simulator used in this study. (b) Schematic illustrations showing the dimensions of the solar simulator.

Α	В	С	D	Α	В	С	D
	10		6		280	275	
:0:	·III	:0		405	<u>2x</u> 325	310	<u>2x</u> 295
: 0	1			420	<u>2x</u> 325	<u>2x</u> 308	<u>2x</u> 300
				<u>4x</u> 325	365	345	520
			0 3-0	450	375	2x 345	525
				470	490	385	525
	.10		0		490	395	

Figure S2: A photograph (left) and schematic representation (right) showing the number and spatial distribution of LEDs on the spherical cap matrix of the photochemical reactor. Each cell contains an LED module, with each module housing up to four LEDs of the same type. The blue rectangle highlights modules connected to the same LED driver.

15 16

17



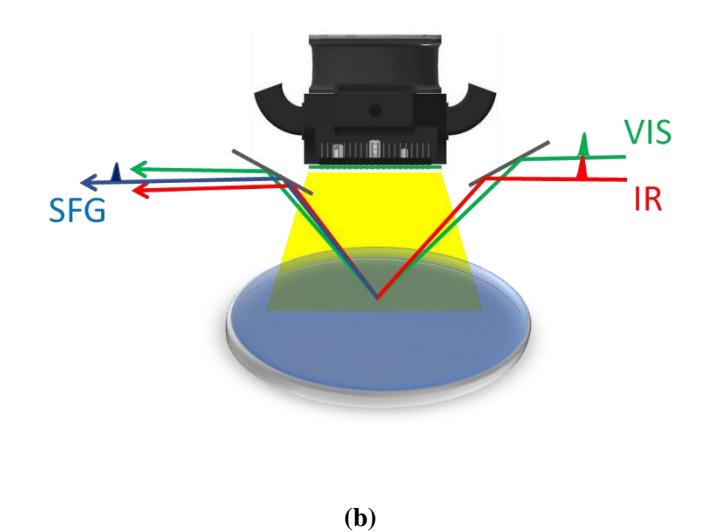
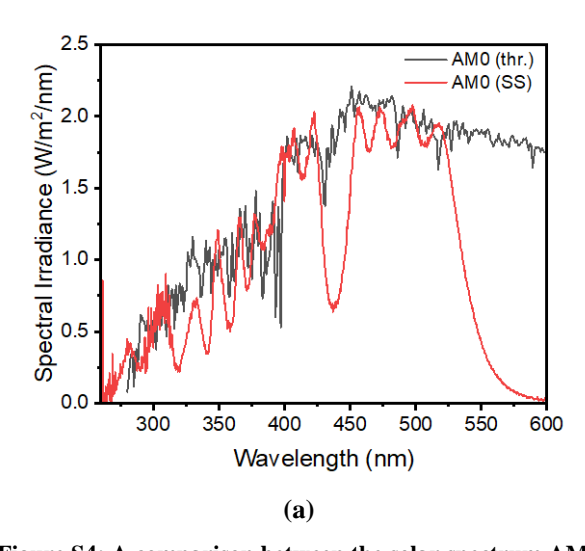


Figure S3: (a) A photograph of the custom-built photochemical reactor mounted above the sample in the SFG setup. (b) A schematic sketch illustrating the sample illumination and SFG ray geometry.

The solar simulator's spectral characteristics were evaluated against AM0 and AM1 solar spectra, calculated using the SMARTS2 code (Gueymard, 1995). Figure S4 compares the simulator's spectral output with these reference spectra. Due to LED availability at the time of construction, a spectral gap exists around 440 nm, and a weaker intensity was achieved near 325 nm. To ensure homogeneity, LEDs with a high divergence angle were selected. The illumination uniformity of an arbitrary power distribution was measured across the sample plane, with intensity variations in the x- and y-directions presented by the shadowed area in Fig. S5. The final configuration allows for spectral adjustments to simulate various atmospheric conditions by modifying LED current biases.





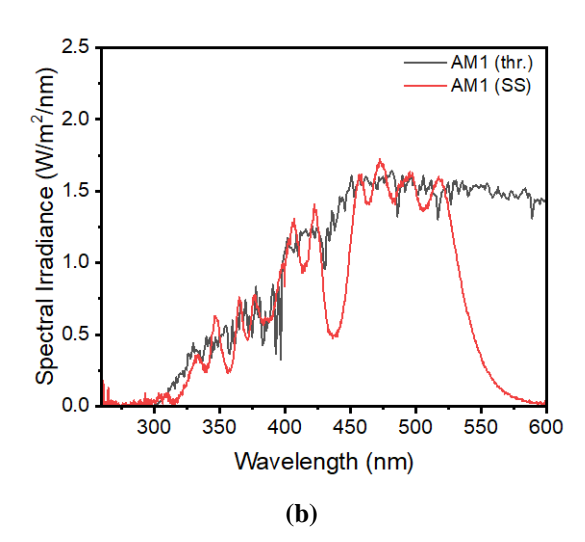
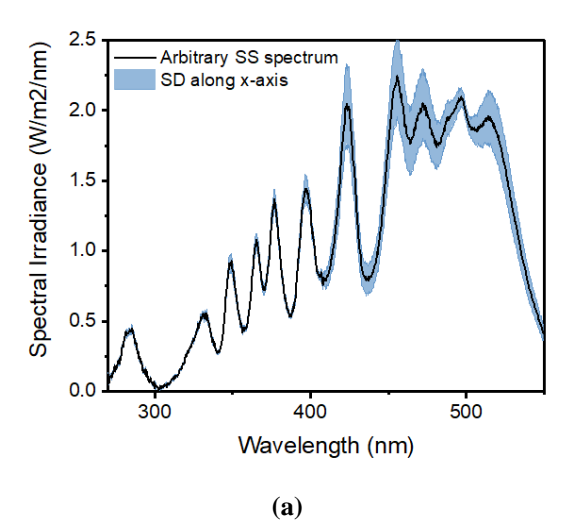
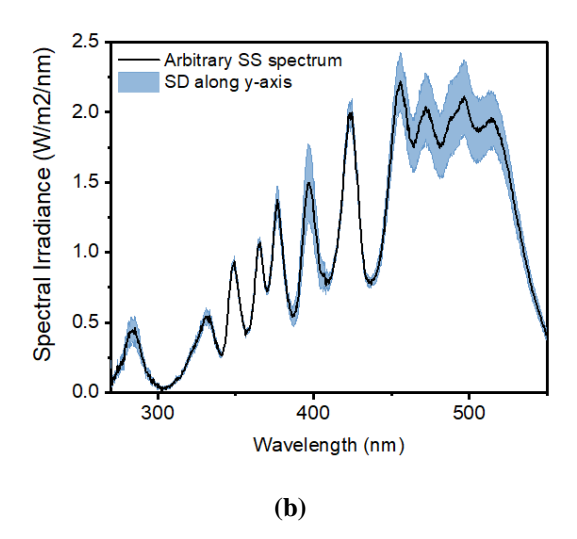


Figure S4: A comparison between the solar spectrum AM0 (a) and AM1 (b) and the corresponding irradiation of the custom-made solar simulator (SS)





- Figure S5: An Arbitrary output spectrum from the SS and intensity variations across the illuminated area in the x- and y-
- 2 directions.

S2. Contamination and purification of 4-BBA

Due to the distinctive characteristic of Sum Frequency Generation (SFG) as a surface-sensitive technique for sub-monolayer analysis, it became apparent that the delivered 4-BBA contained surface-active contaminants. The blue spectrum in Fig. S6 shows vibrational bands in the CH region detected at the air-water interface of a 0.2 mM 4-BBA aqueous solution. These bands are attributed to surface active organic contaminants in the solution. 4-BBA is not surface active (Mora Garcia et al., 2021) and there are no CH bonds that could produce the CH vibrations in SFG spectroscopy. To purify the 4-BBA, it was recrystallized twice from ethanol. The green curve in Fig. S6 shows the SFG spectrum of 4-BBA aquatic solution after the recrystallization. It is worth mentioning that we tested samples from different providers, including the provider mentioned in the reference work (Tinel et al., 2016), and found that 4-BBA was never delivered pure enough to not show surface active contaminants. The contamination in the 4-BBA should be considered when comparing our results with those in the reference work.

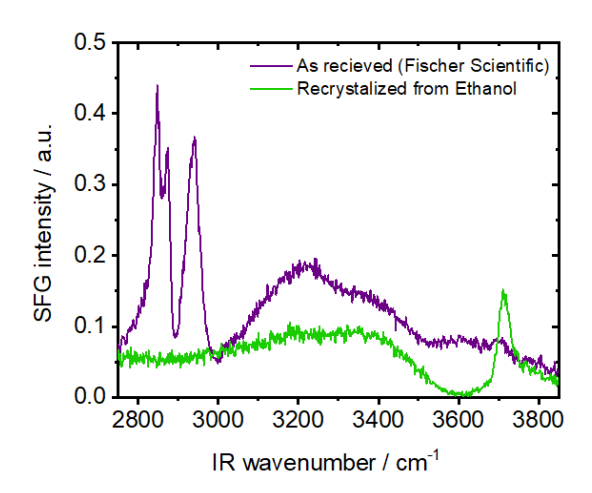


Figure S6: SFG at air-water interface of a 0.2 mM aqueous solution of 4-BBA as received, blue, and after recrystallization twice from Ethanol, green.

1 S3. SFG data and data analysis

2 S3.1. SFG signal

- 3 The SFG signal with frequency $\omega_{SF} = \omega_v + \omega_{IR}$ was collected under SSP polarization (S-polarized
- 4 SFG and VIS; P-polarized IR) generated at the spatial and temporal overlap of the incoming visible
- light with frequency ω_{ν} and infrared light with frequency ω_{IR} . The SFG signal can be described as
- 6 follows:

$$I(\omega_{SF}) \propto \left| \chi_{eff}^{(2)} \right|^2 I_v I_{IR}$$
 (1)

- 7 Where the intensity is proportional to Fresnel factors for reflection and transmission of the
- 8 fundamental and SF beams and an effective second-order nonlinear susceptibility $\chi_{eff}^{(2)}$. To obtain
- 9 peak frequencies and amplitudes the SFG spectra were fitted with a sum of a non-resonant
- contribution, with amplitude A_0 and phase φ , and a sum of Lorentzians for the resonant contribution:

$$I(\omega_{SF}) = \left| \chi_{NR}^{(2)} + \chi_{R}^{(2)} \right|^{(2)} = \left| A_0 e^{i\varphi} + \sum_{q} \frac{A_q}{\omega_{IR} - \omega_q + i\Gamma_q} \right|^{(2)}$$
 (2)

- where A_q , ω_q , and $2\Gamma_q$ are the amplitude, frequency, and full width half maximum linewidth of the
- 12 q^{th} vibrational resonance, respectively.
- Figure S7 shows some examples of the data fitting of the SFG spectra (using the Gnuplot software).
- In each panel, the datapoints represent the raw data, the blue line shows the fitting curve and the
- bright curves below each spectrum show the individual OH, water, and CH bands mentioned in the
- manuscript. The different panels show the spectra of the same mixture (2 mM NA + 0.2 mM 4-BBA
- at pH 8) at different times after mixing the two solutions in dark.

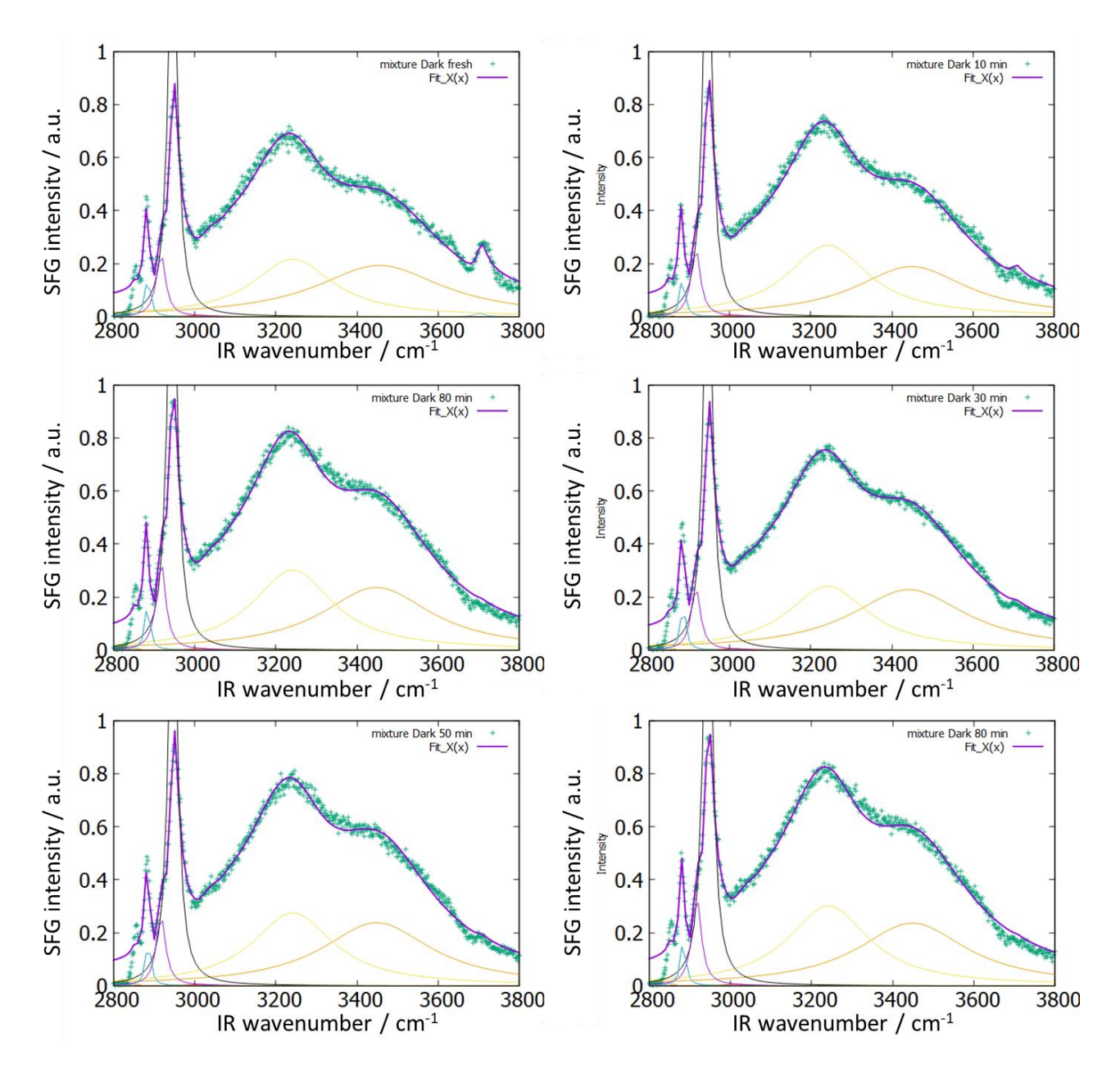


Figure S7: SFG spectra and fitting curves of the mixture (2 mM NA + 0.2 mM 4-BBA) at pH 8 at different times after mixing the two solutions in dark conditions.

S3.2. SFG amplitude change of the individual peaks with time in dark of the

2 mixture (2 mM NA + 0.2 mM 4-BBA) at pH 8

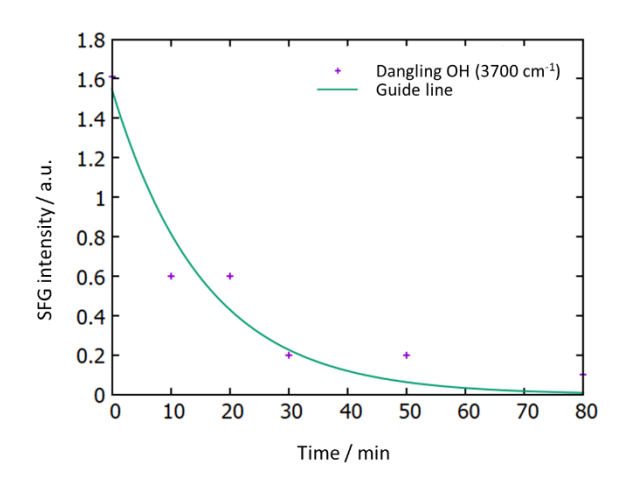


Figure S8: The decay of the dangling-OH SFG peak at the at air - water interface of the mixture at pH = 8 with time in dark conditions.

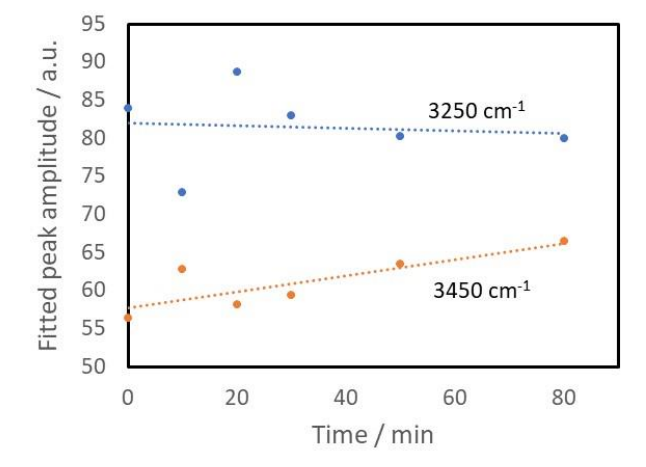


Figure S9: The change of intensity of the two water bands as a function of time in dark conditions at the air – water interface of the mixture at pH 8. The dot lines are guiding lines.

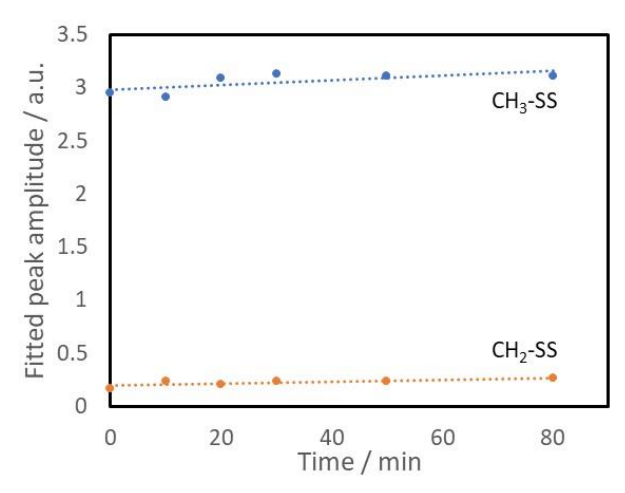
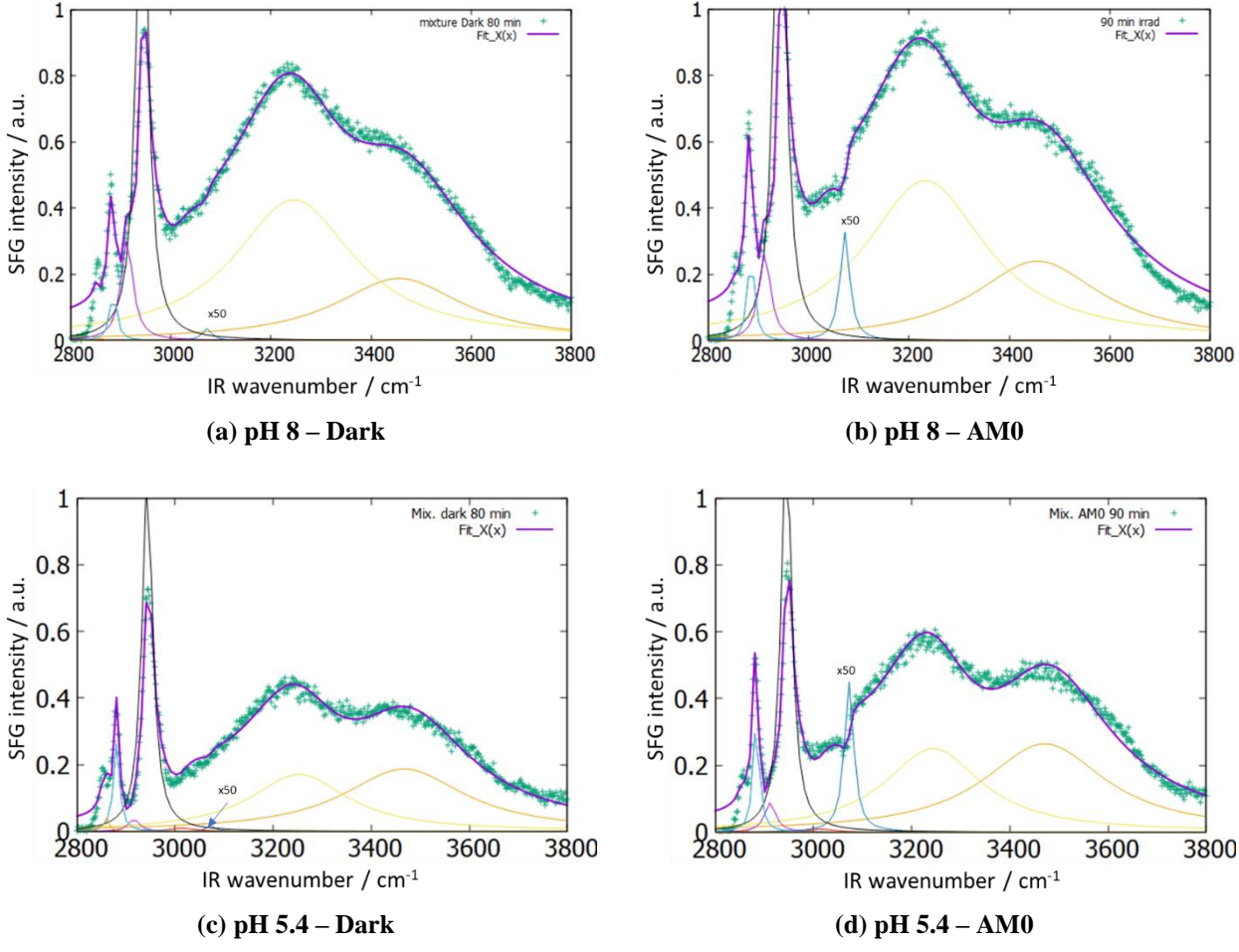


Figure S10. The peak amplitude of CH_3 -SS (blue) and CH_2 -SS as a function of time in dark conditions at the air – water interface of the mixture at pH = 8. The dot lines are guiding lines.

1 S3.3. SFG change of the mixture (2 mM NA + 0.2 mM 4-BBA) after irradiation

2 with different wavelengths



3 Figure S11: SFG spectra and fitting curves of the mixture (2 mM NA + 0.2 mM 4-BBA) at pH 8 and pH 5.4 both before and

⁴ after irradiation with AM0 for 90 min. The aromatic band (at 3070 cm⁻¹) is scaled by x40 for clarity.

1 S3.4. SFG change of the mixture (2 mM NA + 0.2 mM 4-BBA) at pH 5.6 after

2 different irradiation times with different wavelengths

3 4

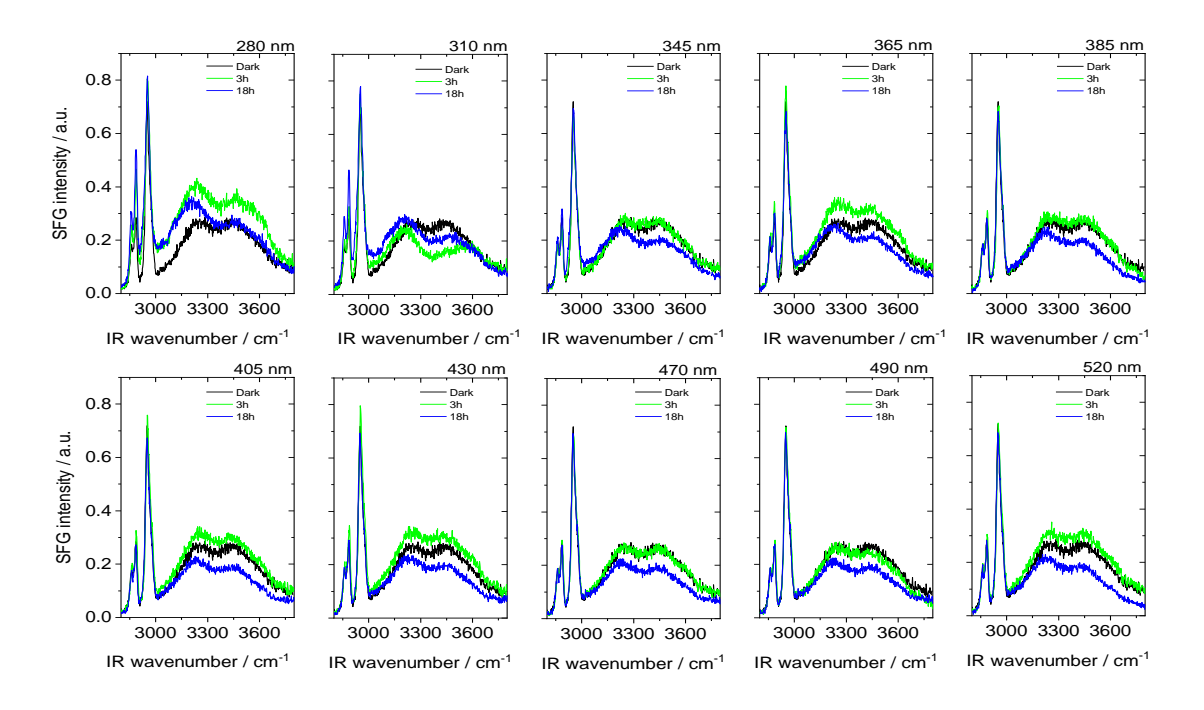


Figure S12: SFG spectra at air-water interface of the mixture (2 mM NA + 0.2 mM 4-BBA) at pH 5.6 after different irradiation times with different wavelengths. A plot without offset. The spectrum after half hour has been omitted for clarity.

S4. Changes of pH with time and UV exposure

High pH solutions undergo a decrease in pH values due to carbonation. In the presence of NA + 4-BBA solution, the decrease in pH was found to be accelerated upon irradiation with UV light. This is obviously due to the contribution of the photogenerated organic compounds. Figure S13a compares the pH change over time for different pH solutions exposed to ambient air immediately after preparation and after the start of UV irradiation (black triangles). In the absence of NA + 4-BBA mixture (red plot), the pH value is constantly decreasing exponentially with time regardless of the illumination condition. In the presence of NA + 4-BBA mixture without irradiation (orange plot), the pH value is also constantly decreasing exponentially with time. However, the rate of decrease in pH for the mixture increases after starting irradiation with UV (gray and blue lines). Finally, the irradiation shows no influence on the pH of the mixture that was prepared at low pH (green line).

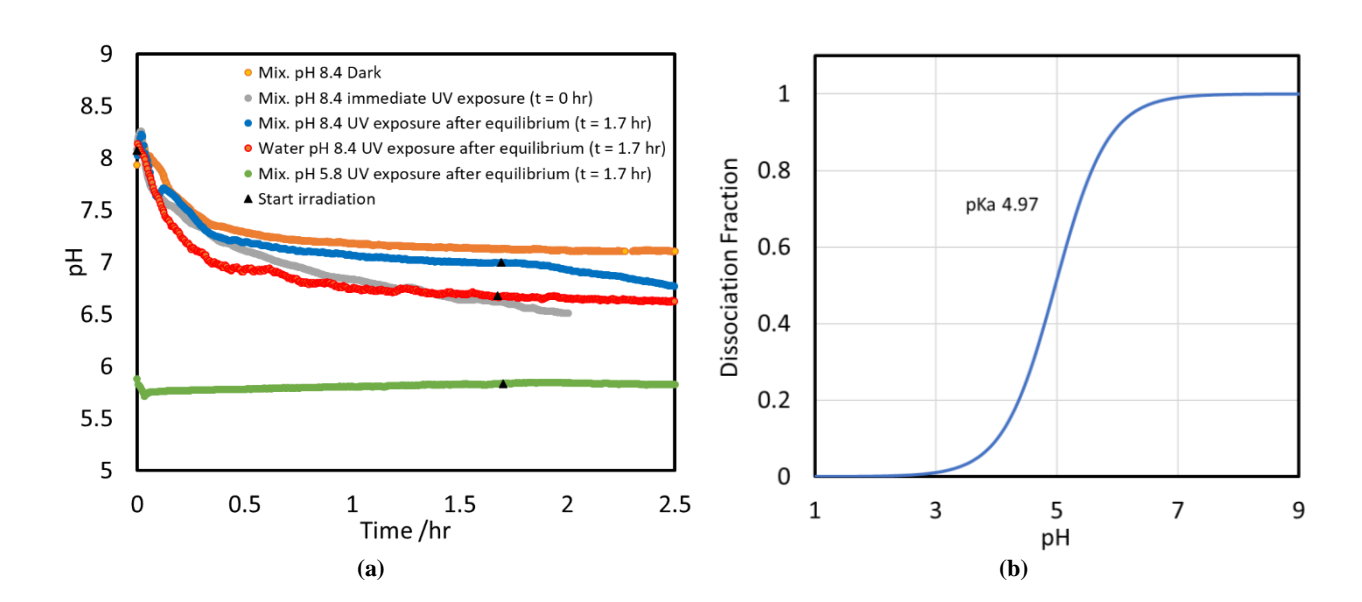


Figure S13: (a) pH-change with time for the mixture prepared at pH 8.4 and kept in dark conditions (orange), the mixture prepared at pH 8.4 and immediately exposed to UV light (gray), the mixture prepared at pH 8.4 and kept in dark to reach equilibrium after approximately 1.7 h before starting exposure to UV light (blue), water adjusted at pH 8.4 and kept in dark to reach equilibrium after approximately 1.7 h before starting exposure to UV light (red), and the mixture prepared at pH 5.8 and kept in dark for approximately 1.7 h before starting exposure to UV light (green). The black triangles indicate the point where the UV lamp (280 nm) was switched ON. (b) Dissociation fraction of NA as a function of pH calculated by Henderson–Hasselbalch equation using pKa = 4.97 (Luo et al., 2020; Wellen et al., 2017).

For the solution with a high pH, a faster decrease in pH in the presence of the mixture (NA + 4-BBA) after switching the UV light on. Under UV light irradiation, the 4-BBA molecule absorbs energy, leading to excitation. The 4-BBA reaction is expected to be a reduction of the carbonyl group which is less likely to happen (Calvert and Pitts, 1966). The NA, however, is more likely to undergo decarboxylation, as a major pathway, as expected for an aliphatic organic acid. Indeed, some major

products observed are C8. The carbonation process is primarily influenced by the concentration of dissolved CO₂ in water and the partial pressure of CO₂ in the surrounding atmosphere. The pH of the solution can indirectly affect carbonation by influencing the equilibrium between carbonic acid and its dissociation products. The fast decrease in pH value under UV light for a solution with an initial ~pH 8 and containing the mixture is a laboratory issue due to the relatively high NA and 4-BBA concentration in a limited sample volume. In nature, this effect is negligible, e.g. in large water reservoirs, but could become relevant, e.g. for cloud droplets.

1

2

3

4

5

6

7

8

9

10

11

12

13

14

15

16

17

18

19

20

21

22

23

24

25

26

To understand the indirect effect of pH change on the SFG signal, we have to recall that the balance between the hydrophobic tail and the hydrophilic head controls the adsorption of surfactants. While hydrophobicity is directly connected with hydrocarbon length, hydrophilicity is mostly unquantified (Rosen and Kunjappu, 2012). The hydrophilicity of head groups is qualitatively related to the solvation and solubility. Thus, a nonionized state would be less hydrophilic than an ionized state because it would be less soluble. NA is partially dissociated in a wide range of pH values (see Fig. S13b). The higher the pH, the higher the dissociation fraction of NA and the lower its surface activity, and vice versa. The change in pH at a constant concentration of NA changes the concentration of NA at the surface and hence the surface pressure (Luo et al., 2020). Although the relationship between the surface pressure and the SFG signal at the air-water interface is not well established, it is confirmed that the SFG signal may increase or decrease with surface pressure depending on a number of factors, such as the composition and arrangement of the molecules at the interface, the polarization of the incident light, and the concentration of adsorbed species (Feng et al., 2016). Finally, solutions of 4-BBA at different pH values change their absorbance spectra due to protonation-deprotonation effect (Karimova et al., 2023), Fig. S14. This increases the complexity of the photoreaction if the pH value is not constant during the irradiation process.

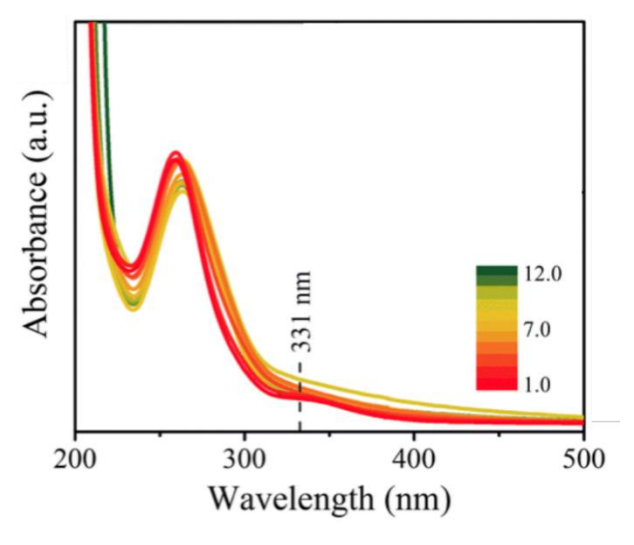


Figure S14: UV-vis absorption spectra of 100 μ M 4-BBA solutions across a pH range of 1.0 to 12.0. Data adapted from (Karimova et al., 2023).

S5 Salt effect (preliminary results)

2

3

4

5

6

7

8

9

10

11

12

13

14

15

16 17

18

19 20 The mineral concentration in bodies of water can impact both salinity and pH levels, which in turn can significantly influence the chemical and physical processes occurring within them, including the photochemistry at the air-water interface. We conducted a preliminary experiment to assess the impact of salinity on the photo-reaction of the system under study. We prepared artificial sea water the Table S1following recipe in taken from: "http://cshprotocols.cshlp.org/content/2012/2/pdb.rec068270.full." Results showed that the presence of salt content accelerated the photo-reaction, as evidenced by the early appearance of the aromatic band (at 3067 cm⁻¹) just 30 minutes after irradiation with AM0 light, compared to the solution without salt. Figure S15 depicts the development of the aromatic band and water bands over time during 14 h of AM0 irradiation. While the exact explanation for this effect is unclear, it is possible that the salt increases the concentration of 4-BBA at the surface, leading to an acceleration of the photoreaction rate. Further investigation of the mechanism under salty conditions is necessary and recommended for future studies.

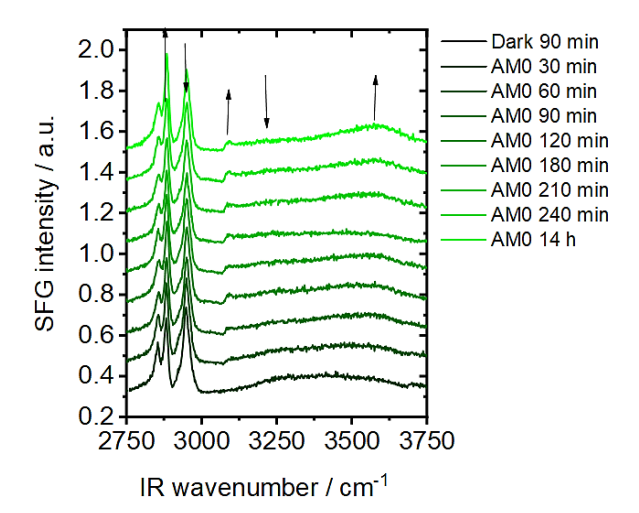


Figure S15: SFG spectra at the air-water interface of the mixture (2 mM NA + 0.2 mM 4-BBA) using artificial seawater at pH 5.4, irradiated with AM0 for 14 h.

Table S1: Artificial sea water recipe

Reagent	Quantity (for 1L)	Final concentration	
NaCl	26.29 g	450 mM	
KCl	0.74 g	10 mM	
CaCl ₂	0.99 g	9 mM	
MgCl ₂ .6H ₂ O	6.09 g	30 mM	
MgSO ₄ .7H ₂ O	3.94 g	16 mM	

S6. Experiment tables

1

4 5 6

7

Table S2: Summary of SFG experimental conditions. All experiments were conducted at a constant temperature of 296 K and a pressure
of 1 atm.

Experiment	Irradiation	NA (mM)	4-BBA (mM)	pН	Gas	Figure
SFG_NA_D_8	Dark	2	0	8	Synthetic air	1a
SFG_NA_L0_8	AM0	2	0	8	Synthetic air	1a
SFG_H2O_D_8	Dark	0	0	8	Synthetic air	1b
SFG_BBA_D_8	Dark	0	0.2	8	Synthetic air	1b
SFG_BBA_L0_8	AM0	0	0.2	8	Synthetic air	1b
SFG_Mix_D_8	Dark	2	0.2	8	Synthetic air	2a
SFG_Mix_L0_8	AM0	2	0.2	8	Synthetic air	2b
SFG_Mix_D_5.4	Dark	2	0.2	5.4	Synthetic air	3a
SFG_Mix_L0_5.4	AM0	2	0.2	5.4	Synthetic air	3b
SFG_Mix_L02_5.4	AM0	2	0.2	5.4	Synthetic air	5a
SFG_Mix_L1_5.4	AM1	2	0.2	5.4	Synthetic air	5b
SFG_Mix_UV_5.4	UV(AM1)	2	0.2	5.4	Synthetic air	5c
SFG_Mix_wl*_5.6	wl*	2	0.2	5.6	Lab air	6, S12

w1* = 280, 310, 345, 365, 385, 405, 430, 470, 490, 520 nm (10 experiments)

Table S3: Summary of MS experimental conditions. All experiments were conducted at a constant temperature of 296 K and a pressure of 1 atm.

Experiment	Irradiation	NA (mM)	4-BBA (mM)	pН	Gas	Figures	
MS_BG1	AM0	0	0	6.2	Crosthatia aim	14	
MIS_DG1	AMU	0	0	0.2	Synthetic air	14	
MS_BG2	AM0	2	0	5.8	Synthetic air	Background for NA	
MS_BG3	AM0	0	0.2	5.8	Synthetic air	Background for 4-BBA	
MS.1	AM0	2	0.2	5.8	Synthetic air	7, 8, 11, 10, 14, 13	
MS.2	AM1	2	0.2	5.8	Synthetic air	10, 11, 13, 14	
MS.3	AM0	2	0.2	5.8	N_2	9, 10, 13	
MS.4	285 nm	2	0.2	5.8	Synthetic air	10, 12, 13, 14	
MS.5	310 nm	2	0.2	5.8	Synthetic air	10, 12, 13, 14	
MS.6	365 nm	2	0.2	5.8	Synthetic air	10, 12, 13, 14	
MS.7	405 nm	2	0.2	5.8	Synthetic air	10, 12, 13, 14	
MS.8	Natural	2	0.2	5.8	Ambient air	10 11 12	
	sunlight	2	0.2		Amoient air	10, 11, 13	

1 S7. Chemical composition of liquid and gas phase

- 2 From MS measurements we can deduct the molar mass and maybe the structural formula but not the
- 3 exact molecule structure. For example, there are many possibilities to draw C₉H₁₆O₄. For this reason,
- 4 we do not suggest names of the photoproducts or show the molecular structures in the manuscript,
- 5 but just the formula corresponding to the molar mass. In Tables S4 and S5, we list some molecules
- 6 that are more likely to form. Figure S16 shows the proposed chemical structures and photolysis
- 7 mechanism of NA in the presence of 4-BBA. Table S6 presents the compounds reported by Tinel et
 - al. (2016) in the gas and liquid phases, along with those that were also detected in our study.
 - Table S4: Main compounds detected in the liquid phase during the MS experiments, with those also reported by Tinel et al. (2016)
- indicated (\checkmark) .

8

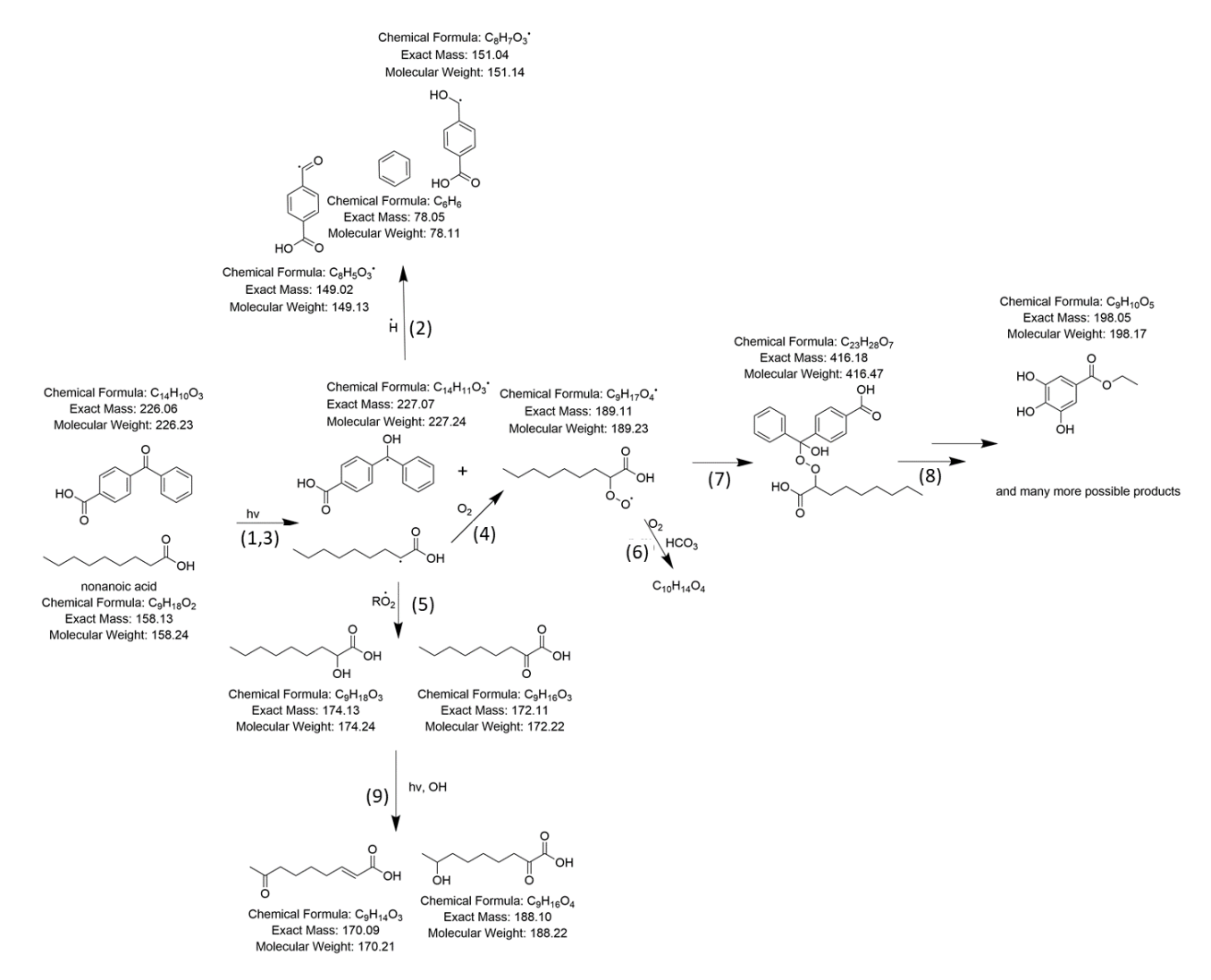
m/z	Tentative formula	Tentative assignment	Tentative structure	Tinel et al. 2016
170.0939	C ₉ H ₁₄ O ₃	Dendryphiellic acid	НО	
172.0732	C ₈ H ₁₂ O ₄	Dioxooctanoic acid	OHO HO	
172.1095	C ₉ H ₁₆ O ₃	Oxononanoic acid	OH OH	√
188.0681	C ₈ H ₁₂ O ₅	Oxooctanedioic acid	но	
188.1044	C ₉ H ₁₆ O ₄	2-Hydroxy-6- oxononanoic acid	0 H O H	✓
198.0525	C ₉ H ₁₀ O ₅	Ethyl Gallate (Ethyl 3,4,5- Trihydroxybenzoate)	HO CH ₃	
198.0888	$C_{10}H_{14}O_4$	Diacetic acid	HO O O O	

1 Table S5. Main compounds detected in the gas phase during the MS experiments, with those also reported by Tinel et al. (2016)

2 indicated (\checkmark) .

3

Mass/z	Formula	Tentative assignment	Tentative structure	Tinel et al. 2016
56.0624	C ₄ H ₈	Butene		✓
72.0573	C ₄ H ₈ O	Butanal		√
70.078	C ₅ H ₁₀	Pentene		√
86.0729	C ₅ H ₁₀ O	Pentanal		√
77.039	C ₆ H ₅	C		
78.0468	C_6H_6	Benzene		
90.0468	C ₇ H ₆	Co		
92.0624	C ₇ H ₈	Toluene		
106.0417	C7H6O	Benzaldehyde		
128.1197	C ₈ H ₁₆ O	Octanal	·//	√



3 Figure S16: Proposed chemical structures with pathways for the photolysis mechanism of NA in the presence of 4-BBA

- Table S6: The molecular formulas of compounds reported by Tinel et al. (2016) in the gas and liquid phases, along with those that were
- 2 also detected in our study.

	Gas phase p	oroducts	Condensed pha	se products
Formula	Tinel et al. 2016	This work	Tinel et al. 2016	This work
C ₃ H ₄ O	√		√	
C ₃ H ₆ O	√		√	
C ₄ H ₆ O	√		√	
C ₄ H ₆ O ₂	✓		√	
C ₄ H ₈	√	√		
C ₄ H ₈ O	√	√	✓	
C ₄ H ₈ O ₂	✓			
C5H8O	√		✓	
C5H8O2	✓		√	
C5H10	√	✓		
C5H10O	√	√	✓	
C5H10O2	√	<u> </u>	·	
C ₆ H ₁₀ O	·		√	
C ₆ H ₁₀ O ₂	·		·	
C ₆ H ₁₂	√		,	
C ₆ H ₁₂ O	·		√	
C ₆ H ₁₂ O ₂	·		,	
C ₇ H ₁₂ O	√		✓	
C7H12O2	•		√	
C7H14O	√		√	
C7H14O2	V		√	
C ₈ H ₁₄ O	√		√	
C8H14O2	V		√	
C8H14O2			√	
C8H14O3			√	
C8H16	√		V	
C ₈ H ₁₆ O	√	√	/	
C8H16O2	V	V	√ √	
			√	
C8H16O3 C8H16O4			· ·	
C9H14O4			√ √	
C9H16O	/			
C9H16O2	√ √		√ √	
	+		+	
C9H16O3 C9H16O4	√		√ /	<u>√</u>
C9H16O4 C9H18	,		√	√
	√ 		,	
C ₂ H ₁₈ O	√		√ 	
C9H18O3			√ /	
C9H18O4			√ /	
C II O			√ 	
C II O			√	
C ₂₃ H ₂₈ O ₅			√ ,	
C ₂₇ H ₅₀ O ₆			√ ,	
C28H22O6			√	

 $[\]checkmark$: Detected compound.

Table S7: The error values for the pie charts of Fig. 14.

Species	err							
C8H12O4	0.018	0.021	0.074	0.025	0.02	0.021	0.04	0.05
C8H12O5	0.006	0.003	0.004	0.003	0.002	0.003	0.003	0.003
C9H10O5	0.051	0.035	0.009	0.05	0.062	0.05	0.014	0.012
C9H14O3	0.006	0.005	0.006	0.002	0.004	0.005	0.004	0.004
C9H16O3	0.043	0.062	0.045	0.055	0.05	0.057	0.07	0.065
C9H16O4	0.005	0.006	0.005	0.003	0.003	0.004	0.003	0.003
C10H14O4	0.009	0.01	0.005	0.009	0.008	0.008	0.008	0.008
Other	0.01	0.012	0.011	0.01	0.01	0.011	0.015	0.01

1 References

- 2 Calvert, J. G. and Pitts, J. N.: Photochemistry, 2nd ed., Wiley, New York, USA, 730 pp., 1966.
- 3 Feng, R.-J., Li, X., Zhang, Z., Lu, Z., and Guo, Y.: Spectral assignment and orientational analysis in a
- 4 vibrational sum frequency generation study of DPPC monolayers at the air/water interface, J. Chem. Phys.,
- 5 145, 244707, https://doi.org/10.1063/1.4972564, 2016.
- 6 Gueymard, C.: SMARTS2: A Simple Model of the Atmospheric Radiative Transfer of Sunshine:
- 7 Algorithms and Performance Assessment, Florida Solar Energy Center, Cocoa, Florida, 1995.
- 8 Karimova, N., Alija, O., Mora García, S. L., Grassian, V. H., Gerber, R. B., and Navea, J. G.: pH
- 9 Dependence of the speciation and optical properties of 4-benzoylbenzoic acid, Phys. Chem. Chem. Phys., 25,
- 10 17306–17319, https://doi.org/10.1039/D3CP01520C, 2023.
- Luo, M., Wauer, N. A., Angle, K. J., Dommer, A. C., Song, M., Nowak, C. M., Amaro, R. E., and Grassian,
- 12 V. H.: Insights into the behavior of nonanoic acid and its conjugate base at the air/water interface through a
- combined experimental and theoretical approach, Chem. Sci., 11, 10647–10656,
- 14 https://doi.org/10.1039/D0SC02354J, 2020.
- Mora Garcia, S. L., Pandit, S., Navea, J. G., and Grassian, V. H.: Nitrous Acid (HONO) Formation from the
- 16 Irradiation of Aqueous Nitrate Solutions in the Presence of Marine Chromophoric Dissolved Organic Matter:
- 17 Comparison to Other Organic Photosensitizers, ACS Earth Sp. Chem., 5, 3056–3064,
- https://doi.org/10.1021/acsearthspacechem.1c00292, 2021.
- 19 Rosen, M. J. and Kunjappu, J. T.: Surfactants and interfacial phenomena, John Wiley & Sons, 2012.
- Tinel, L., Rossignol, S., Bianco, A., Passananti, M., Perrier, S., Wang, X., Brigante, M., Donaldson, D. J.,
- and George, C.: Mechanistic Insights on the Photosensitized Chemistry of a Fatty Acid at the Air/Water
- 22 Interface, Environ. Sci. Technol., 50, 11041–11048, https://doi.org/10.1021/acs.est.6b03165, 2016.
- Wellen, B. A., Lach, E. A., and Allen, H. C.: Surface pK a of octanoic, nonanoic, and decanoic fatty acids at
- 24 the air-water interface: applications to atmospheric aerosol chemistry, Phys. Chem. Chem. Phys., 19, 26551-
- 25 26558, https://doi.org/10.1039/C7CP04527A, 2017.